Local atomic geometry and Ti 1*s* near-edge spectra in $PbTiO_3$ and $SrTiO_3$

Eric Cockayne,[1,*] Eric L. Shirley,[2,†] Bruce Ravel,[1] and Joseph C. Woicik[1]

[1]*Materials Measurement Science Division, Material Measurement Laboratory, National Institute of Standards and Technology, Gaithersburg, Maryland 20899, USA*

[2]*Sensor Science Division, Physical Measurement Laboratory, National Institute of Standards and Technology, Gaithersburg, Maryland 20899, USA*

(Received 19 March 2018; published 31 July 2018)

We study Ti 1*s* near-edge spectroscopy in $PbTiO_3$ at various temperatures above and below its tetragonal-to-cubic phase transition, and in $SrTiO_3$ at room temperature. *Ab initio* molecular dynamics (AIMD) runs on 80-atom supercells are used to determine the average internal coordinates and their fluctuations. We determine that one vector local order parameter is the dominant contributor to changes in spectral features: the displacement of the Ti ion with respect to its axial O neighbors in each Cartesian direction, as these displacements enhance the cross section for transitions to E_g-derived core-hole exciton levels. Using periodic five-atom structures whose relative Ti-O displacements match the root-mean-square values from the AIMD simulations, and core-hole Bethe-Salpeter equation calculations, we quantitatively predict the respective Ti 1*s* near-edge spectra. Properly accounting for atomic fluctuations greatly improves the agreement between theoretical and experimental spectra. The evolution of relative strengths of spectral features vs temperature and electric field polarization vector are captured in considerable detail. This work shows that local structure can be characterized from first-principles sufficiently well to aid both the prediction and the interpretation of near-edge spectra.

DOI: 10.1103/PhysRevB.98.014111

I. INTRODUCTION

Perovskite ABO_3 compounds are a family of materials of technological interest, in part because of their usefulness as dielectric and piezoelectric materials. A variety of phase transitions are seen in perovskite oxides, from ferroelectric transitions in $BaTiO_3$ and $PbTiO_3$ to antiferrodistortive transitions in $SrTiO_3$ and more complicated transitions in $CaTiO_3$ and $PbZrO_3$. Additionally, *relaxor* behavior[1–3] (a broad, frequency-dependent dielectric maximum vs temperature, not associated with a paraelectric-ferroelectric phase transition) can occur in perovskite solid solutions such as $Pb[Mg_{1/3}Nb_{2/3}]O_3$ (PMN).

Many of the practical properties of these materials are due to the displacement of ions in response to temperature, electric fields, stress, etc. Response functions can also be related to fluctuations and correlations of the ionic positions over time and/or space [4,5]. To clarify structure-property relationships, it is therefore important to fully characterize the ionic positions as a function of temperature, etc., not only the average positions, but also their fluctuations around the average over time and/or unit cells. Such distributions can reveal interesting features that can dramatically affect a material's properties, such as characteristic deviations of local structure from the average. While a difference between local atomic geometries and average properties is naturally expected in complex perovskites where different species occupy the same crystallographic site, pioneering work of Comes *et al.* [6] gave evidence that even simple perovskites such as $BaTiO_3$ and $KNbO_3$ in their cubic phases can exhibit correlated off-centering of their B ions (e.g., Ti or Nb).

There are many theoretical methods to determine local atomic geometries in materials. Density-functional theory (DFT) ground-state calculations are direct, but are limited regarding the sizes of systems that can be treated. Also, DFT calculations are usually restricted to the zero-temperature case, and are subject to systematic error because of approximate treatments of exchange and correlation. To overcome the DFT zero-temperature problem, DFT-based *ab initio* molecular dynamics (AIMD) calculations allow finite-temperature fluctuations of ionic coordinates to be incorporated in the Born-Oppenheimer limit. However, the sizes of treatable systems may be even further restricted, and one must cover a sufficiently long simulation time to equilibrate to representative conditions at a given temperature. A molecular dynamics calculation that uses first-principles-based effective Hamiltonians or force-field models allows for effects involving greater length and timescales to be investigated, but its predictions are generally not as accurate as those obtained using AIMD.

There are also many experimental methods to determine local atomic geometry [7]. For example, x-ray absorption fine structure spectroscopies [near-edge x-ray absorption fine structure (NEXAFS), also known as x-ray absorption near-edge structure (XANES), and extended x-ray absorption fine structure (EXAFS)] can furnish a wealth of information via interference effects because of a core-level photoelectron's multiple scattering from atomic sites [8]. Such core level spectroscopies are element-specific, and the excitonic "pre-edge" features (involving 1*s*-to-3*d* transitions from the ground state to a bound core-hole exciton state) are strongly affected

*eric.cockayne@nist.gov
†eric.shirley@nist.gov

by variations in the B site (e.g., Ti) position with respect to its nearest neighbors. As an example, this effect was previously demonstrated in strained, thin-film ferroelectric $SrTiO_3$ [9]. In that work, x-ray diffraction and DFT determination of the unit cell size and internal atomic coordinates agreed with respect to the detailed crystal structure, and theoretical and experimental NEXAFS calculations indicated similar degrees of Ti off-centering in the TiO_6 cages. Bulk calculations confirmed selection rules for excitation into T_{2g} and E_g core-hole exciton levels, and these rules were violated in a fashion that is consistent with average displacements and thermal fluctuations of the Ti coordinate relative to its O_6 cage.

Lead titanate ($PbTiO_3$) is a compound of interest, in part because it is an end member of important solid solutions, such as lead-zirconium titanate (PZT). It has a single tetragonal/cubic transition at $T = 763$ K, with the cubic phase existing at higher temperatures. At room temperature, the Ti 1*s* near-edge spectrum in $PbTiO_3$ features an E_g peak near 4970.5 eV that is strongly enhanced compared to the T_{2g} peak for x-ray photon electric field polarization along the tetragonal axis [9]. This is a hallmark signature of Ti off-centering relative to the surrounding O_6 octahedra in the tetragonal phase. However, the peak is still enhanced in the cubic phase above the transition temperature, whereas Bethe-Salpeter equation (BSE) calculations that assume only *average* cubic perovskite structure fail to predict this enhancement. Instead, thermal fluctuations must be taken into account [10]. Related EXAFS studies [11,12] also indicate off-centering of Pb and Ti in $PbTiO_3$ above the transition temperature.

In this work, we combine AIMD and a BSE treatment of the Ti 1*s* near-edge spectrum in a fashion that addresses the thermal fluctuations. We find that the important fluctuations for a given temperature can be effectively reproduced by a single periodic five-atom cell. BSE calculations are performed using these cells and compared with measured spectra [10] to investigate the local structure in $PbTiO_3$ as a function of temperature and in $SrTiO_3$ at room temperature.

In what follows, we review the background and theoretical methodology (i.e., AIMD and BSE calculations). Aspects of measurements of experimental spectra to which we compare results are given in more detail elsewhere [10]. We then present our results, comparing calculated and measured spectra, and present our conclusions, primarily that our present accounting of ionic fluctuations greatly improves agreement between theoretical and measured spectra in the pre-edge region.

II. BACKGROUND AND METHODOLOGY

A. Underlying physics

Let a Ti 1*s* electron's coordinate relative to the nucleus be denoted by **r**. Then the effective light-matter interaction operator responsible for a core excitation can be approximated as

$$\hat{O} \approx (\mathbf{e}\cdot\mathbf{r}) + \frac{i}{2}(\mathbf{e}\cdot\mathbf{r})(\mathbf{q}\cdot\mathbf{r}). \quad (1)$$

Here, **e** is the photon's electric-field polarization vector, and **q** is its wave vector. Thus, the vectors **q** and **e** determine how the two terms, respectively, allow electric dipole (E1) and quadrupole (E2) transitions at the Ti 1*s* near edge. As a consequence, a variety of experimental parameters can be varied to "tease out" and assign various spectral features, depending on the orientations of **e** and **q** relative to the crystallographic directions, as well as temperature, film thickness, polarization, strain, and flexure. Near-edge spectra in $SrTiO_3$ and $PbTiO_3$ reveal electric-dipole and electric-quadrupole transitions to Ti 4*p*, 3*d*, and mixed 4*p*-3*d* states. Weak, crystal-field-split "pre-edge" features are attributed to $1s \rightarrow 3d$ transitions and are small compared to the main "edge jump" at the onset of the Ti 4*p* continuum states around and above 4970 eV.

For octahedral Ti site symmetry, there are two leading pre-edge features, around 4968.5 eV and 4970.5 eV, because the T_{2g} and E_g orbitals are separated by the ligand-field splitting. These are understood as excitation to the 3*d* level on the same site as the 1*s* hole, while the next features around 4974 eV could arise from excitation to 3*d* levels on nearby Ti sites because of hybridization with the on-site 4*p* states mediated by the O 2*p* states [10,13]. In the presence of a Ti 1*s* core hole, an electron in any of the on-site orbitals would be bound to the Ti site, so that the electron-core hole pair constitutes a core-hole exciton. Pseudo-Jahn-Teller splittings and site symmetry lower than cubic symmetry can split the otherwise threefold and twofold degeneracies further. The edge jump is chiefly due to the E1 term, which can greatly enhance pre-edge features when Ti-site inversion symmetry is broken. In that case, low lying Ti 4*p*-derived and 3*d*-derived E_g states, which are close in energy, mix, so that the latter become more strongly accessible via the E1 term. Otherwise, the E2 term alone can give rise to the weak pre-edge features. Selection rules imply that 3*d* lobes should have projections in the plane of **e** and **q** but not along either of these vectors. As an example, the antiferrodistortive tetragonal phase of $SrTiO_3$ should affect the E2 selection rules regarding observation of d_{xy}-derived vs $d_{x^2-y^2}$-derived exciton levels when **e** and **q** are both in the basal plane because of TiO_6 cage rotations. However, fluctuations of the cage rotational angles about their average values can be substantial, further weakening the selection rules. As examples of past work in the near-edge spectroscopy of simple perovskites, Ti off-centering in $PbTiO_3$ was analyzed by Vedrinskii *et al.* [10] and Ravel *et al.* [14], and Ti off-centering in $SrTiO_3$ by several groups [9,15]. Other effects of symmetry were studied theoretically and experimentally in non-perovskite compounds containing TiO_6 cages, such as rutile and anatase [16–18].

B. *Ab initio* molecular dynamics calculations

From the theory in Sec. II A, the physics that dominates the Ti near edge in $PbTiO_3$ and $SrTiO_3$ involves Ti ions and their nearest O neighbors. The pertinent local environment thus features seven atoms: the Ti itself and an octahedron of six surrounding O ions. Under O_h symmetry, the 21 corresponding vibrational degrees of freedom transform into irreproducible representations (irreps) as follows: $a_{1g} + e_g + t_{1g} + t_{2g} + 3\,t_{1u} + t_{2u}$. One displacement pattern for each irrep is given in Fig. 1. and the corresponding normalized full displacement patterns are given in Table S1 of the Supplemental Material [19]. In the most important local displacement pattern in this work $t_{1u}^{(1)}(z)$, the central Ti ion moves proportionally to $+(\sqrt{2/3})c$ along z and the two neighboring O ions in the $\pm z$ direction move proportionally to $-(\sqrt{1/6})c$ along z, where c

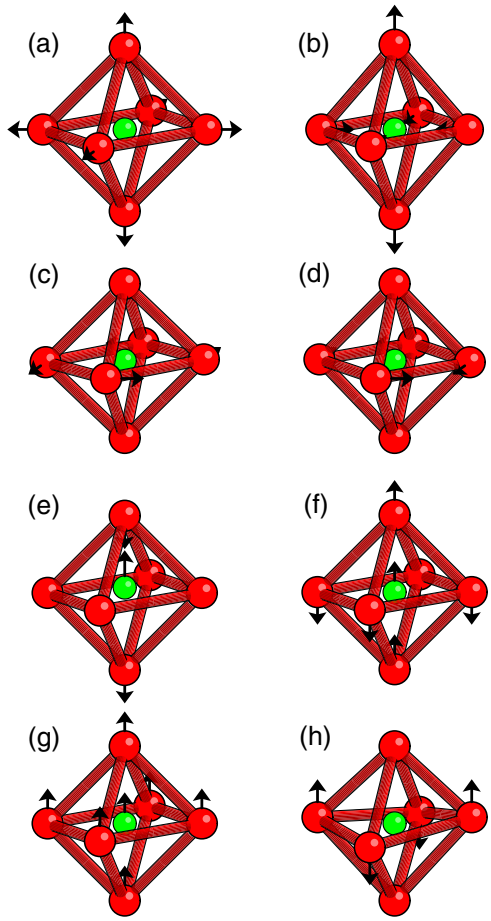

FIG. 1. One component of each irreducible representation for local TiO_6 distortions in a cubic titanate perovskite: (a) a_{1g}; (b) $e_g(z)$; (c) $t_{1g}(z)$; (d) $t_{2g}(z)$; (e) $t_{1u}^{(1)}(z)$; (f) $t_{1u}^{(2)}(z)$; (g) $t_{1u}^{(3)}(z)$; (h) $t_{2u}(z)$. Some "away-pointing" arrows are obscured.

is the lattice parameter of the primitive five-atom perovskite cell along z (see Table I). For the corresponding $t_{1u}^{(1)}(x)$ and $t_{1u}^{(1)}(y)$ patterns, z is replaced by $x(y)$ and c is replaced by a. For simplicity, the same mode labels are used here for cubic and for tetragonal $PbTiO_3$; tetragonal cell modes are identified with the cubic irrep from which they are derived.

Ab initio molecular dynamics [20] using DFT at the generalized-gradient-approximation (GGA) level with Hubbard U corrections was used to compute the time varying atomic coordinates $x_{\mu i}(t)$. Here, t denotes time, μ labels one of the above 21 local modes, and i the position (unit cell). Simulations were run for $PbTiO_3$ at 300 K, 600 K, and 900 K. For all runs, we used 80-atom supercells with lattice vectors (0,2,2), (2,0,2), and (2,2,0) in terms of the lattice vectors of the corresponding five-atom primitive perovskite cell. The MD was run using the Vienna *Ab initio* Simulation Package (VASP) code [21,22]. The simulation time step was 1.25 fs, and the total simulation time was 2.5 ps (2000 time steps). Langevin dynamics were used, with a frequency of 2 THz. The final runs were performed after a series of initialization runs totaling 2 ps. Such a simulation time is relatively short compared to other AIMD studies of $PbTiO_3$ [23,24], because we enforced high convergence with respect to k points and plane-wave cutoff energy. Nevertheless, the 2.5-ps run is sufficient for convergence of atomic coordinate averages and fluctuations, as found by consistency of the results of the final run with those of the previous 1.25-ps initialization run.

It is well known that the GGA gives a c/a ratio for $PbTiO_3$ that is much larger than experiment [25]. We have found empirically that the PBEsol [26] GGA with a Hubbard correction of $U = 2.3$eV for oxygen p states and an artificial pressure of -21 kbar (-2.1 GPa) reproduces low-temperature structures of other perovskite titanates such as $BaTiO_3$, $CaTiO_3$, and $SrTiO_3$ quite well, but the c/a ratio of $PbTiO_3$ remains too high. (It has recently been suggested that the inclusion of van der Waals forces, neglected here, can strongly affect the calculated c/a ratio [27].) On the other hand, we find that a room-temperature AIMD run for $PbTiO_3$ with the above parametrization, and with the unit cell fixed at the experimental one, yields an average structure with ionic positions within 0.05 Å of the experimental values. Therefore, each AIMD run was performed with the primitive lattice parameters fixed at the experimental values at the corresponding temperature [28,29]. The lattice constants used are presented in Table II.

Defining $\langle Q\rangle_t$ as an average of quantity Q over time and $\langle Q\rangle_i$ as an average over sites, we define the mode average of a local coordinate by its mean value, namely,

$$\overline{x_\mu} = \langle\langle x_{\mu i}(t)\rangle_i\rangle_t, \tag{2}$$

and the root-mean-square local coordinate as

$$\sigma(\mu) = \left(\left\langle\left\langle x_{\mu i}^2(t)\right\rangle_i\right\rangle_t\right)^{1/2}. \tag{3}$$

We also define the time-and-space deviation of a coordinate from its mean value by $x'_{\mu i}(t) = x_{\mu i}(t) - \overline{x_\mu}$. Most of the mode averages $\overline{x_\mu}$ are zero by symmetry. However, in the tetragonal $PbTiO_3$ phase, the average amplitudes of the polar $t_{1u}(z)$ modes are nonzero.

TABLE I. Atomic displacements corresponding to unit amplitude of the $t_{1u}^{(1)}(z)$ degree of freedom for the TiO_6 cluster in a perovskite titanate. Entries that are zero are left blank. The unit-amplitude $t_{1u}^{(1)}(x)$ and $t_{1u}^{(1)}(y)$ displacement patterns can be found by cyclic permutation and by replacing the z direction five-atom primitive perovskite cell lattice parameter c with the corresponding lattice parameter in the x or y direction. Atomic displacement patterns for the other TiO_6 cluster degrees of freedom can be found in Table S1 of the Supplemental Material [19].

Ti			O_{+x}			O_{-x}			O_{+y}			O_{-y}			O_{+z}			O_{-z}		
x	y	z	x	y	z	x	y	z	x	y	z	x	y	z	x	y	z	x	y	z
		$(2/\sqrt{6})c$															$(-1/\sqrt{6})c$			$(-1/\sqrt{6})c$

TABLE II. Experimental lattice parameters for $SrTiO_3$ and $PbTiO_3$ [28,29] used in this work (in Å).

	$SrTiO_3$	$PbTiO_3$		
T(K)	293	300	600	900
a	3.9051	3.901	3.927	3.980
c	3.9051	4.157	4.099	3.980

C. Bethe-Salpeter equation calculations

In Sec. II B, we describe the 21 degrees of freedom of a TiO_6 unit, and how their averages and root-mean squares were calculated via AIMD. Before discussing the details of our Bethe-Salpeter equation calculations, we determine which of these 21 degrees of freedom are important. Rigid translation of the TiO_6 cage ($t_{1u}^{(3)}$ modes) has no effect on the absorption spectrum, while rigid rotation (t_{1g}) serves only to change the polarization selection rules for E2 transitions. Of the remaining 15 degrees of freedom, isotropic breathing (a_{1g}) has little impact on the spectrum, while the two e_g breathing modes are responsible for pseudo-Jahn-Teller splitting of the $1s$-to-E_g peak [30,31]. The t_{2g}, $t_{1u}^{(2)}$, and t_{2u} modes do not change Ti-O distances to first order. Thus, the set of three $t_{1u}^{(1)}$ modes in which the Ti ion moves relative to its axial O neighbors are expected to dominate the near-edge spectra. Furthermore, the spectra should be proportional to the square of the amplitude of the mode. Thus, averaging over unit cells, the expected spectra are equivalent to that for a single periodic five-atom cell where the amplitude of each component of the $t_{1u}^{(1)}$ displacement pattern is equal to the corresponding root-mean-square value over all cells. Explicit expressions for the effective atomic coordinates, valid for $ATiO_3$ perovskites of cubic and tetragonal symmetry, are given in Table III. The A_z and O_z displacements in Table III under tetragonal symmetry are insignificant (for near-edge spectra purposes), but are set at their values determined from the average AIMD structure.

In our calculations, we chose to have the c axis along the z direction. Two x-ray photon geometries were considered, corresponding to what was measured. One geometry had $\mathbf{q} \parallel (-1, -1, 0)$ and $\mathbf{e} \parallel (0, 0, 1)$, and one geometry had $\mathbf{q} \parallel (0, -1, 1)$ and $\mathbf{e} \parallel (1, 0, 0)$. Randomization of signs of displacements along each Cartesian direction was incorporated by averaging spectra with suitable variation of the signs of Cartesian components of $\mathbf{q}$ and $\mathbf{e}$.

The x-ray absorption coefficient can be given as

$$\mu(E) = -\mathrm{Im}\langle\Phi_0|\hat{O}^\dagger \frac{1}{E + i\Gamma(E) - H}\hat{O}|\Phi_0\rangle, \qquad (4)$$

where Φ_0 denotes the ground state, $\Gamma(E)$ accounts for lifetime damping of excited states, and H is the effective Hamiltonian for the electron core-hole pair's equation of motion, which is the Bethe-Salpeter equation. This Hamiltonian includes effects of the band structure, electron self-energy damping calculated as described elsewhere [32], core hole lifetime damping [33], and the very important screened electron-core hole interaction. The Bethe-Salpeter equation solver is described by Vinson *et al.* [34], with various details regarding the calculation of matrix elements given elsewhere [35].

A precursor DFT calculation underlies the BSE calculation. This provides Bloch state wave functions and energies. We used a 200 Ry plane-wave cutoff. This was necessary to describe Ti $3s$ and $3p$ states well, while simultaneously having Ti $4s$ and $4p$ energies sufficiently accurate by virtue of a hard pseudopotential for Ti. Thus, we used He-like, Ne-like, and Hg^{2+}-like cores for Vanderbilt-type pseudopotentials [36] for O, Ti, and Pb, respectively. We used the local-density approximation [37] with the Ceperley-Alder functional [38] as parametrized by Perdew and Zunger [39]. The self-consistent charge density was found using $4 \times 4 \times 4$ Monkhorst-Pack grids [40].

The BSE calculation includes 155 bands total and $10 \times 10 \times 10$ grids. This was accelerated by use of optimized basis functions described by Prendergast and Louie [41], who improved upon earlier work [42]. The electron-core hole interaction was screened as described elsewhere [43]. For the electronic dielectric constant, we used $\epsilon_\infty = 7.25$ at $T = 300$ K, $\epsilon_\infty = 7.60$ at $T = 600$ K, $\epsilon_\infty = 8.68$ at $T = 900$ K, which averages the values of the three diagonal elements of the measured dielectric tensor at each temperature [44].

III. RESULTS AND DISCUSSION

The average crystallographic structures found in the AIMD simulations are given in Table IV, while the root-mean-square fluctuations of the important $t_{1u}^{(1)}$ modes are given in Table V. An example of how the local $t_{1u}^{(1)}(z)$ coordinate for one specific Ti ion varies over time for different temperatures is shown in Fig. 2. Normalization of the $t_{1u}^{(1)}(z)$ displacement pattern (Table I) means that the displacement of the Ti relative to the

TABLE III. Coordinates of five-atom structures for use in the Bethe-Salpeter equations to compute near-edge spectra of cubic or tetragonal simple $ATiO_3$ perovskites, given root-mean-square fluctuations associated with the t_{1u} local coordinate (Table I). The origin is chosen such that the crystallographic average position of one O atom is (0.5, 0.5, 0.0). A_z and O_z coordinates are set at their average values.

	$T = 300$ K		
Ion	x	y	z
A	0	0	A_z
Ti	$0.5 + (2/\sqrt{6})\,\sigma(t_{1u}^{(1)}(x))$	$0.5 + (2/\sqrt{6})\,\sigma(t_{1u}^{(1)}(y))$	$0.5 + (2/\sqrt{6})\,\sigma(t_{1u}^{(1)}(z))$
O	$0.0 - (1/\sqrt{6})\,\sigma(t_{1u}^{(1)}(x))$	0.5	O_z
O	0.5	$0.0 - (1/\sqrt{6})\,\sigma(t_{1u}^{(1)}(y))$	O_z
O	0.5	0.5	$0.0 - (1/\sqrt{6})\,\sigma(t_{1u}^{(1)}(z))$

TABLE IV. Temperature-dependent average structure of $PbTiO_3$ from AIMD.

	$T = 300$ K		
Ion	x	y	z
Pb	0.0000	0.0000	0.1056
Ti	0.5000	0.5000	0.5709
O	0.0000	0.5000	0.4982
O	0.5000	0.0000	0.4982
O	0.5000	0.5000	0.0000
	$T = 600$ K		
Ion	x	y	z
Pb	0.0000	0.0000	0.0739
Ti	0.5000	0.5000	0.5550
O	0.0000	0.5000	0.4993
O	0.5000	0.0000	0.4993
O	0.5000	0.5000	0.0000
	$T = 900$ K		
Ion	x	y	z
Pb	0.0000	0.0000	0.0000
Ti	0.5000	0.5000	0.5000
O	0.0000	0.5000	0.5000
O	0.5000	0.0000	0.5000
O	0.5000	0.5000	0.0000

neighboring oxygens in the $\pm z$ directions is $3/\sqrt{6} \times c$ times the amplitude shown in this figure.

A histogram of the amplitudes of the $t_{1u}^{(1)}(z)$ fluctuations of *all* Ti atoms versus temperature is shown in Fig. 3. For $T = 900$ K, we additionally show the histogram of displacements obtained by symmetrizing the data over $\pm z$. The asymmetry in the "raw" data is attributed to insufficient averaging time in the 2.5-ps AIMD run. Interestingly, at all temperatures investigated, the peak amplitude of the $t_{1u}^{(1)}$ fluctuation is similar: about 0.1, or about a 0.5-Å relative displacement of Ti against O along the z direction.

There are two possibilities for the behavior in the cubic phase above the ferroelectric transition at $T = 763$ K: if the amplitude peaks at zero, that indicates a displacive nature to the Ti off-centering in the ferroelectric transition; if the amplitude has two peaks at nonzero values, that indicates an order-disorder nature of Ti off-centering. Our present results for $T = 900$ K cannot clearly distinguish between the two cases. It would be useful to repeat the AIMD calculation for temperatures closer to the transition temperature, but the correlation length and time of the Ti off-centering fluctuation are expected to increase as the phase transition is approached [4,45], requiring larger simulations cells and times for convergence. Our AIMD simulations used 80-atom cells. Classical molecular dynamics based on a bond-valence-sum model for $PbTiO_3$ has recently been used to simulate cells with up to 2560 atoms [46]. Determining the fluctuations of the $t_{1u}^{(1)}$ modes via the classical MD approach could help clarify to what extent the root-mean-square local fluctuations are affected by longer-range correlations near the transition temperature.

Experimentally, near-edge measurements reported by Yoshiasa *et al.* [12] on a $PbTiO_3$ powder sample show a nearly continuous evolution of the intensity of the E_g-derived peak near the transition temperature, suggesting a smooth trend

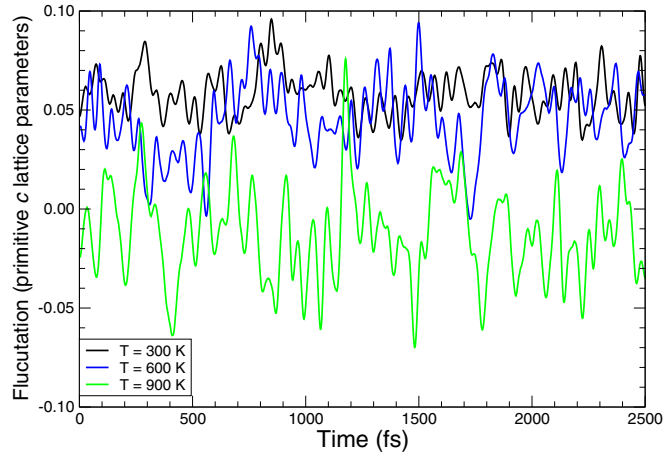

FIG. 2. $t_{1u}^{(1)}(z)$ fluctuation of one Ti against its $\pm z$ oxygen neighbors vs MD time, at different temperatures.

TABLE V. Root-mean-square fluctuations $\sigma(\mu)$ of the $t_{1u}^{(1)}$ modes of $PbTiO_3$ as a function of temperature, as computed by *ab initio* molecular dynamics. Quantities in parentheses indicate one standard deviation uncertainty as calculated from five time averages. To convert into atomic displacements, multiply by the displacement patterns described in Table I. Root-mean-square fluctuations for the other modes as a function of temperature can be found in Table S2 of the Supplemental Material [19].

	$\sigma(\mu)$		
Mode μ	300 K	600 K	900 K
$t_{1u}^{(1)}(x;y)$	0.0138(1)	0.0207(4)	0.0294(3)
$t_{1u}^{(1)}(z)$	0.0592(1)	0.0495(4)	0.0294(3)

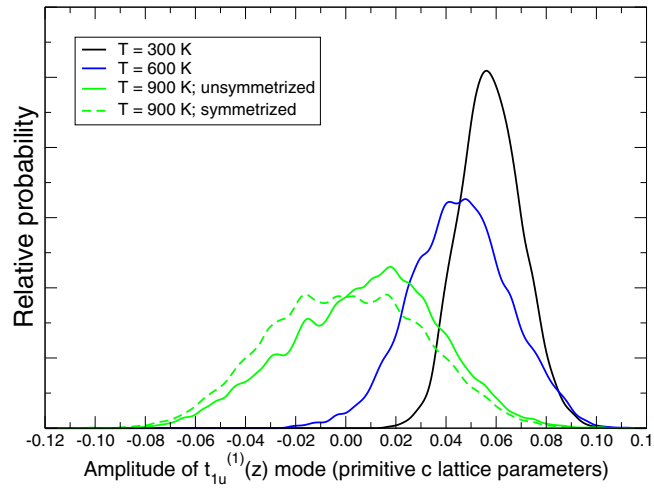

FIG. 3. Histograms of amplitude of $t_{1u}^{(1)}(z)$ fluctuation of Ti ions against their $\pm z$ O neighbors in $PbTiO_3$ versus temperature, as calculated via *ab initio* molecular dynamics. The raw data for $T = 900$ K is shown, as well as the data symmetrized about zero.

TABLE VI. Structures used in the Bethe-Salpeter equations to compute near-edge spectra in $PbTiO_3$. These are *not* the average crystallographic structures at the corresponding temperature, but are specifically created such that Ti is off-centered along each coordinate by the root-mean-square fluctuation as calculated by AIMD simulations.

	$T = 300$ K		
Ion	x	y	z
Pb	0.0000	0.0000	0.1056
Ti	0.5113	0.5113	0.5483
O	0.9944	0.5000	0.4982
O	0.5000	0.9944	0.4982
O	0.5000	0.5000	0.9758
	$T = 600$ K		
Ion	x	y	z
Pb	0.0000	0.0000	0.0739
Ti	0.5169	0.5169	0.5404
O	0.9915	0.5000	0.4993
O	0.5000	0.9915	0.4993
O	0.5000	0.5000	0.9798
	$T = 900$ K		
Ion	x	y	z
Pb	0.0000	0.0000	0.0000
Ti	0.5240	0.5240	0.5240
O	0.9880	0.5000	0.5000
O	0.5000	0.9880	0.5000
O	0.5000	0.5000	0.9880

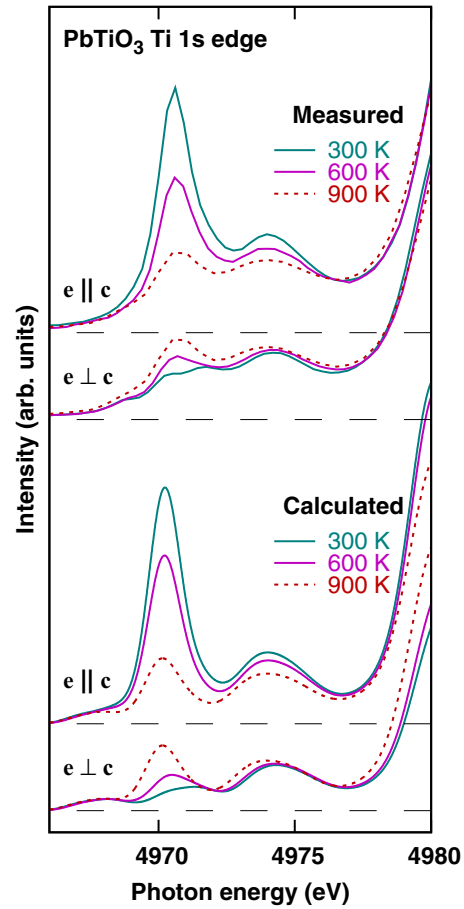

FIG. 4. Ti 1*s* near-edge spectrum emphasizing the pre-edge region for $PbTiO_3$ at three temperatures, as measured and calculated.

for the root-mean-square Ti off-centering vs temperature, but measurement of a root-mean-square off-centering by itself does not show whether the underlying distribution has one peak or two. Other experimental [11] and computational [24] studies of $PbTiO_3$ support an order-disorder nature of the phase transition in $PbTiO_3$. Neither of these studies measured precisely the same "local order parameter" as the AIMD calculations in this work. In light of our results, this raises the intriguing question of whether different possible local order parameters for the tetragonal-cubic transition in $PbTiO_3$ could give different answers for the displacive vs order-disorder nature of the transition.

Plugging the AIMD fluctuations for $PbTiO_3$ (Table V) into the general expression formula for the effective five-atom cell for BSE calculations (Table III), yields the temperature-dependent effective structures given in Table VI. Based on these effective structures, computed near-edge spectra for each x-ray photon geometry are presented in Fig. 4 for three temperatures for $PbTiO_3$ and compared to measured spectra. The spectra are vertically offset for presentation, with the baseline indicated by a dashed line in each case. It should be noted that a rigid shift was required to energetically align the spectra, which is standard practice for calculated core excitation spectra. The peak that betrays the T_{2g}-derived core hole-exciton levels near 4968.5 eV shows minimal dependence on either temperature or x-ray photon geometry. On the other hand, the corresponding peak for E_g-derived levels near 4970.5 eV shows a strong dependence on temperature. For $\mathbf{e} \perp (001)$, it grows in strength with temperature because of admixture of the Ti 4*p* and Ti $3d_{x^2-y^2}$ levels because of fluctuations of the Ti *x* and *y* coordinates. However, this peak becomes particularly pronounced for $\mathbf{e} \parallel (001)$ at temperatures below the transition temperature, when Ti off-centering is largest, especially at lower temperatures. A broad feature around 4974 eV appears to be enhanced along with the E_g-derived feature. Off-centering of the Ti affects hybridization of Ti 4*p* and O 2*p* states. In the unoccupied bands, there should be a node in such an antibonding state between the Ti and O atoms, and the weight of the Ti 4*p* state on the Ti site can be enhanced because of increasing localization arising from the node and foreshortened bond length [10,13].

In addition to $PbTiO_3$, we show results for $SrTiO_3$ obtained at $T = 293$ K [9]. In this case, the two x-ray photon geometries that were considered were (i) $\mathbf{q} \parallel (1, 1, 0)$ and $\mathbf{e} \parallel (1, -1, 0)$, and (ii) $\mathbf{q} \parallel (1, 0, 0)$ and $\mathbf{e} \parallel (0, 1, 0)$. Naïvely, the first geometry should make transitions to Ti $3d_{x^2-y^2}$-derived core hole-exciton levels observable, though not transitions to Ti $3d_{xy}$-derived core hole-exciton levels. For the second geometry, exactly the opposite should hold true. In fact, while the selection rule works nearly perfectly for the T_{2g}-derived peak, the E_g-derived peak is always visible with similar intensity in either case. We performed similar calculations in $SrTiO_3$ as described for $PbTiO_3$. AIMD simulations $SrTiO_3$ at room temperature give fluctuations $\sigma(t_{1u}^{(1)}) = 0.0141$ along

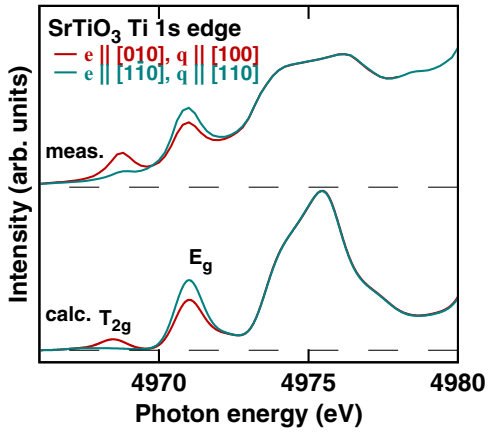

FIG. 5. Ti 1*s* near-edge spectrum emphasizing the pre-edge region for $SrTiO_3$ at 293 K, as measured and calculated.

each Cartesian direction. The resulting spectra are shown in Fig. 5. Good agreement between the theoretical and experimental results is again observed, and the figure suggests similar breakdowns of selection rules being observed and calculated. Violations of selection rules have also been found that allow $s \rightarrow s$ transitions in x-ray absorption because of lattice vibrations, which has been reported by others [47–50]. We also note that the exaggerated intensity of the features near 4975 eV in $SrTiO_3$ could result from the BSE calculation's failure to account for charge-transfer processes that should appear like more effect screening of the Ti 1*s* hole when the excited core electrons leave the Ti site [51].

IV. CONCLUSIONS

This work considers Ti 1*s* near-edge spectroscopic signatures of atomic displacement from those of the ideal perovskite structure in $PbTiO_3$ (and $SrTiO_3$) for a variety of sample temperatures and experimental geometries. Using a combination of AIMD and BSE calculations, we have found that only one type of mode has a strong spectroscopic signature, namely the $t_{1u}^{(1)}$ degrees of freedom involving the Ti^{4+} moving relative to its axial O neighbors. This permits having the BSE calculations sample only a few frozen configurations of atomic coordinates to estimate effects on spectra accurately. To a good approximation, the strong peak around 4970.5 eV varies as the mean-square displacement of this mode, and therefore does not vanish above the ferroelectric-paraelectric transition temperature, even though the average structure has Ti at the center of its oxygen cage.

Our results show that AIMD and BSE can be combined to successfully demonstrate the local fluctuations of Ti in $PbTiO_3$ and suggest that similar analysis could be fruitfully applied in other systems such as relaxors. We have not attempted to consider cage-rotation effects at low temperature in $SrTiO_3$. In that case, the associated modes could be both low frequency and considerably more anharmonic, which might require extensions beyond the present analysis. In earlier work, a single, consistent picture could be constructed regarding crystal structure and local atom geometries based on several methods, including x-ray diffraction, x-ray absorption, density-functional theory calculations of ground-state structures, and the degree and directionality of ferroelectric polarization and/or local off-centering in several perovskites [9,52]. This work now incorporates molecular dynamics into the suite of collectively consistent and compatible methodologies in the same systems.

[1] L. Eric Cross, Relaxorferroelectrics: An overview, Ferroelectrics **151**, 305 (1994).
[2] A. A. Bokov and Z.-G. Ye, Recent progress in relaxor ferroelectrics with perovskite structure, J. Mater. Sci. **41**, 31 (2006).
[3] R. A. Cowley, S. N. Gvasaliya, S. G. Lushnikov, B. Roessli, and G. M. Rotaru, Relaxing with relaxors: a review of relaxor ferroelectrics, Adv. Phys. **60**, 229 (2011).
[4] K. M. Rabe and E. Cockayne, Temperature-dependent dielectric and piezoelectric response of ferroelectrics from first principles, in *First-Principles Calculations for Ferroelectrics*, Vol. 436 (AIP Conference Proceedings, Melville, 1998), pp. 61–70.
[5] I. Ponomareva, L. Bellaiche, T. Ostapchuk, J. Hlinka, and J. Petzelt, Terahertz dielectric response of cubic $BaTiO_3$, Phys. Rev. B **77**, 012102 (2008).
[6] R. Comes, M. Lambert, and A. Guinier, The chain structure of $BaTiO_3$ and $KNbO_3$, Solid State Commun. **6**, 715 (1968).
[7] S. J. L. Billinge and I. Levin, The problem with determining atomic structure at the nanoscale, Science **316**, 561 (2007).
[8] J. J. Rehr and A. L. Ankudinov, Progress in the theory and interpretation of XANES, Coord. Chem. Rev. **249**, 131 (2005).
[9] J. C. Woicik, E. L. Shirley, C. S. Hellberg, K. E. Andersen, S. Sambasivan, D. A. Fischer, B. D. Chapman, E. A. Stern, P. Ryan, D. L. Ederer, and H. Li, Ferroelectric distortion in $SrTiO_3$ thin films on Si (001) by x-ray absorption fine structure spectroscopy: Experiment and first-principles calculations, Phys. Rev. B **75**, 140103 (2007).
[10] R. V. Vedrinskii, V. L. Kraizman, A. A. Novakovich, Ph. V. Demekhin, and S. V. Urazhdin, Pre-edge fine structure of the 3d atom K x-ray absorption spectra and quantitative atomic structure determinations for ferroelectric perovskite structure crystals, J. Phys.: Condens. Matter **10**, 9561 (1998).
[11] N. Sicron, B. Ravel, Y. Yacoby, E. A. Stern, F. Dogan, and J. J. Rehr, Nature of the ferroelectric phase transition in $PbTiO_3$, Phys. Rev. B **50**, 13168 (1994).
[12] A. Yoshiasa, T. Nakatani, T. Hiratoko, T. Tobase, A. Nakatsuka, M. Okube, H. Arima, and K. Sugiyama, Temperature dependence of Zr and Ti K-edge XANES spectra for para- and ferro-electric perovskite-type $PbZrO_3$, $PbTiO_3$, and $BaTiO_3$, J. Phys.: Conf. Series **712**, 012121 (2016).
[13] F. de Groot, G. Vankó, and P. Glatzel, The 1s x-ray absorption pre-edge structures in transition metal oxides, J. Phys.: Condens. Matter **21**, 104207 (2009).
[14] B. Ravel, E. A. Stern, Y. Yacobi, and F. Dogan, Lead titanate is not a classic case of a displacive ferroelectric phase-transition, Jpn. J. Appl. Phys. **32**, 782 (1993).
[15] S. Nozawa, T. Iwazumi, and H. Osawa, Direct observation of the quantum fluctuation controlled by ultraviolet irradiation in $SrTiO_3$, Phys. Rev. B **72**, 121101 (2005).

[16] T. Uozumi, K. Okada, A. Kotani, O. Durmeyer, J. P. Kappler, E. Beaurepaire, and J. C. Parlebas, Experimental and theoretical investigation of the pre-peaks at the Ti K-edge absorption spectra in TiO_2, Europhysics Letters (EPL) **18**, 85 (1992).

[17] L. A. Grunes, Study of the *K* edges of 3*d* transition metals in pure and oxide form by x-ray absorption spectroscopy, Phys. Rev. B **27**, 2111 (1983).

[18] O. Durmeyer, J. P. Kappler, E. Beaurepaire, J. M. Heintz, and M. Drillon, Ti K XANES in superconducting $LiTi_2O_4$ and related compounds, J. Phys.: Condens. Matter **2**, 6127 (1990).

[19] See Supplemental Material at http://link.aps.org/supplemental/10.1103/PhysRevB.98.014111 for displacement patterns and fluctuations of all symmetry-adapted TiO_6 degrees of freedom.

[20] M. C. Payne, M. P. Teter, D. C. Allan, T. A. Arias, and J. D. Joannopoulos, Iterative minimization techniques for ab initio total-energy calculations: molecular dynamics and conjugate gradients, Rev. Mod. Phys. **64**, 1045 (1992).

[21] G. Kresse and J. Furthmuller, Efficient iterative schemes for *ab initio* total-energy calculations using a plane-wave basis set, Phys. Rev. B **54**, 11169 (1996).

[22] Certain commercial software is identified in this paper to adequately describe the methodology used. Such identification does not imply recommendation or endorsement by the National Institute of Standards and Technology, nor does it imply that the software identified is necessarily the best available for the purpose.

[23] V. Srinivasan, $PbTiO_3$ at finite temperature: An ab-initio molecular dynamics study, in *AIP Conference Proceedings*, Vol. 677 (AIP, Melville, 2003), p. 168.

[24] H. Fang, Y. Wang, S. Shang, and Z.-K. Liu, Nature of ferroelectric-paraelectric phase transition and origin of negative thermal expansion in $PbTiO_3$, Phys. Rev. B **91**, 024104 (2015).

[25] H. Meštrić, R.-A. Eichel, T. Kloss, K.-P. Dinse, So. Laubach, St. Laubach, P. C. Schmidt, K. A. Schönau, M. Knapp, and H. Ehrenberg, Iron-oxygen vacancy defect centers in $PbTiO_3$: Newman superposition model analysis and density functional calculations, Phys. Rev. B **71**, 134109 (2005).

[26] J. Tao and J. P. Perdew, Test of a nonempirical density functional: Short-range part of the van der Waals interaction in rare-gas dimers, J. Chem. Phys. **122**, 114102 (2005).

[27] K. Berland, C. A. Arter, V. R. Cooper, K. Lee, B. I. Lundqvist, E. Schröder, T. Thonhauser, and P. Hyldgaard, Van der Waals density functionals built upon the electron-gas tradition: facing the challenge of competing interactions, J. Chem. Phys. **140**, 18A539 (2014).

[28] S. A. Mabud and A. M. Glazer, Lattice parameters and birefringence in $PbTiO_3$ single crystals, J. Appl. Cryst. **12**, 49 (1979).

[29] R. W. G. Wyckoff, *Crystal Structures*, 2nd ed., Vol. 2 (John Wiley and Sons, New York, 1964).

[30] S. Tinte and E. L. Shirley, Vibrational effects on $SrTiO_3$ Ti 1s absorption spectra studied using first-principles methods, J. Phys.: Condens. Matter **20**, 365221 (2008).

[31] K. Gilmore and E. L. Shirley, Numerical quantification of the vibronic broadening of the $SrTiO_3$ Ti L-edge spectrum, J. Phys.: Condens. Matter **22**, 315901 (2010).

[32] T. T. Fister, M. Schmidt, P. Fenter, C. S. Johnson, M. D. Slater, M. K. Y. Chan, and Eric L. Shirley, Electronic structure of lithium battery interphase compounds: Comparison between inelastic x-ray scattering measurements and theory, J. Chem. Phys. **135**, 224513 (2011).

[33] M. O. Krause and J. H. Oliver, Natural widths of atomic K-levels and L-levels, K-alpha x-ray-lines and several KLL Auger lines, J. Phys. Chem. Ref. Data **8**, 329 (1979).

[34] J. Vinson, J. J. Rehr, J. J. Kas, and E. L. Shirley, Bethe-Salpeter equation calculations of core excitation spectra, Phys. Rev. B **83**, 115106 (2011).

[35] E. L. Shirley, Ti 1s pre-edge features in rutile: a Bethe-Salpeter calculation, J. Electron Spectrosc. Relat. Phenom. **136**, 77 (2004).

[36] D. Vanderbilt, Optimally smooth norm-conserving pseudopotentials, Phys. Rev. B **32**, 8412 (1985).

[37] W. Kohn and L. J. Sham, Self-consistent equations including exchange and correlation effects, Phys. Rev. **140**, A1133 (1965).

[38] D. M. Ceperley and B. J. Alder, Ground State of the Electron Gas by a Stochastic Method, Phys. Rev. Lett. **45**, 566 (1980).

[39] J. P. Perdew and A. Zunger, Self-interaction correction to density-functional approximations for many-electron systems, Phys. Rev. B **23**, 5048 (1981).

[40] H. J. Monkhorst and J. D. Pack, Special points for Brillouin-zone integrations, Phys. Rev. B **13**, 5188 (1976).

[41] D. Prendergast and S. G. Louie, Bloch-state-based interpolation: an efficient generalization of the Shirley approach to interpolating electronic structure, Phys. Rev. B **80**, 235126 (2009).

[42] Eric L. Shirley, Optimal basis sets for detailed Brillouin-zone integrations, Phys. Rev. B **54**, 16464 (1996).

[43] Eric L. Shirley, Local screening of a core hole: A real-space approach applied to hafnium oxide, Ultramicroscopy **106**, 986 (2006).

[44] W. Kleemann, F. J. Schäfer, and D. Rytz, Crystal optical studies of precursor and spontaneous polarization in $PbTiO_3$, Phys. Rev. B **34**, 7873 (1986).

[45] P. C. Hohenberg and B. I. Halperin, Theory of dynamic critical phenomena, Rev. Mod. Phys. **49**, 435 (1977).

[46] S. Liu, I. Grinberg, H. Takenaka, and A. M. Rappe, Reinterpretation of the bond-valence model with bond-order formalism: An improved bond-valence-based interatomic potential for $PbTiO_3$, Phys. Rev. B **88**, 104102 (2013).

[47] D. Manuel, D. Cabaret, Ch. Brouder, Ph. Sainctavit, A. Bordage, and N. Trcera, Experimental evidence of thermal fluctuations on the x-ray absorption near-edge structure at the aluminum *K* edge, Phys. Rev. B **85**, 224108 (2012).

[48] T. A. Pascal, U. Boesenberg, R. Kostecki, T. J. Richardson, Tsu-Chien Weng, D. Sokaras, D. Nordlund, E. McDermott, A. Moewes, J. Cabana, and D. Prendergast, Finite temperature effects on the x-ray absorption spectra of lithium compounds: First-principles interpretation of x-ray Raman measurements, J. Chem. Phys. **140**, 034107 (2014).

[49] J. Vinson, T. Jach, W. T. Elam, and J. D. Denlinger, Origins of extreme broadening mechanisms in near-edge x-ray spectra of nitrogen compounds, Phys. Rev. B **90**, 205207 (2014).

[50] R. Nemausat, C. Gervais, C. Brouder, N. Trcera, A. Bordage, C. Coelho-Diogo, P. Florian, A. Rakhmatullin, I. Errea, L. Paulatto, M. Lazzeri, and D. Cabaret, Temperature dependence of x-ray absorption and nuclear magnetic resonance spectra: probing quantum vibrations of light elements in oxides, Phys. Chem. Chem. Phys. **19**, 6246 (2017).

[51] J. C. Woicik, C. Weiland, and A. K. Rumaiz, Loss for photoemission versus gain for Auger: Direct experimental evidence of crystal-field splitting and charge transfer in photoelectron spectroscopy, Phys. Rev. B **91**, 201412 (2015).

[52] J. C. Woicik, E. L. Shirley, K. Gilmore, K. E. Andersen, and C. S. Hellberg, Local structural distortions in strained $Ba_{0.5}Sr_{0.5}TiO_3$ thin films, Phys. Rev. B **96**, 104111 (2017).